

Synthesis, Structure and Characterisation of a New Trinuclear Di- μ -phenolato- μ -carboxylato Mn^{III}Mn^{II}Mn^{III} Complex with a Bulky Pentadentate Ligand: Chemical Access to Mononuclear Mn^{IV}-OH Entities

Christelle Hureau,*^[a,b] Elodie Anxolabéhère-Mallart,*^[a] Geneviève Blondin,^[a]
Eric Rivière,^[a] and Martine Nierlich^[c]

Keywords: EPR spectroscopy / Manganese / Mass spectrometry / N,O ligands / Oxidation

A new trinuclear Mn^{III}Mn^{II}Mn^{III} complex has been isolated and X-ray characterised, namely [(py-salpn)Mn^{III}(μ -OAc)-Mn^{II}(μ -OAc)Mn^{III}(py-salpn)]²⁺ (**1**), where H₂py-salpn is the new bulky [N₃O₂] ligand derived from the H₂salpn Schiff base by the addition of one pyridine arm and the reduction of the imine function. The crystal structure reveals that the complex has a strictly 180° Mn^{III}...Mn^{II}...Mn^{III} angle, the Mn^{II} ion being located at an inversion centre. The complex is valence-trapped, with the terminal Mn^{III} ions showing a Jahn-Teller elongation along the pyridine-Mn^{III}-acetate axis. The Mn^{II}...Mn^{III} separation is 3.1224(13) Å. The EPR spectra recorded on solid and frozen solutions are consistent with an

Mn^{III}Mn^{II}Mn^{III} species. The electrochemical response of complex **1** in acetonitrile solution exhibits two, one-electron reduction waves at $E_{1/2} = 0.140$ and -0.075 V vs. SCE. Phenolato and acetato \rightarrow Mn^{III} ligand-to-metal charge-transfer transitions are detected by UV/Visible spectroscopy at 359 and 587 nm, respectively. Chemical oxidation of an acetonitrile solution with *tert*-butyl hydroperoxide leads to mononuclear Mn^{IV}-hydroxo species, as evidenced by UV/Visible and EPR spectroscopy as well as ESI mass spectrometry.

(© Wiley-VCH Verlag GmbH & Co. KGaA, 69451 Weinheim, Germany, 2005)

Introduction

The development of bioinorganic manganese chemistry has been stimulated by the involvement of manganese ions in many biological systems,^[1,2] such as superoxide dismutase,^[3] catalase^[4] and photosystem II of green plants.^[5–8] In this last intricate machinery, an oxomanganese entity is the key element of the oxygen evolving complex (OEC), which performs the light-induced oxidation of water into dioxygen. This reaction requires the photogeneration of four oxidative equivalents and their storage by the OEC. These two processes are accomplished during the first four steps of the Kok cycle,^[9,10] (S₀→S₁, S₁→S₂, S₂→S₃ and S₃→S₄) where S_{*i*} (*i* = 0–4) denote the five oxidation states of the OEC, dioxygen being released during the last step (S₄→S₀). High-valent oxidation states are thus reached by the manganese ions in the S₄ state. Recently, two X-ray structures obtained for the photosystem II (PSII) of the cyanobacte-

rium *Thermosynechococcus elongatus* have appeared in the literature, one at 3.5 Å^[11] and the other at 3.2 Å resolution.^[12] The structure of the Mn cluster, however, is still a matter of debate. Nevertheless, the resolution level allows the authors to propose two models of the OEC that agree in terms of having two moieties: a small one containing one cation and a larger one containing three or more cations. Zouni et al. describe the OEC cluster as containing only four metal ions, whereas Ferreira et al. describe the oxomanganese entity as a “3+1” tetranuclear manganese complex. More precisely, in the latter case three manganese ions together with one calcium ion are arranged in a tetrahedral geometry at four corners of a distorted cube, the other four corners being occupied by bridging oxo ions. The fourth manganese ion is linked to the Mn-Ca-oxo cube by a unique oxo bridge. Two amino acid residues are involved in the coordination of the fourth manganese ion, namely Asp170 and Glu333, and Asp61 is coordinated through a water molecule. Lastly, one exogenous labile hydrogencarbonate ligand is proposed to interact with the fourth manganese and the calcium ions. Due to its peculiar location and to the presence in its surroundings of labile positions along with the tightly bound Ca²⁺, this fourth manganese ion is anticipated to ensure a special role in the water oxidation process. In particular, the present structure supports recent hypotheses in which one of the four manganese ions binds a water molecule, thus producing a highly reactive intermediate. This electrophilic species is then predisposed

[a] Laboratoire de Chimie Inorganique, UMR 8613, LCR-CEA no. 33V, Institut de Chimie Moléculaire et des Matériaux d'Orsay, Université Paris Sud, 91405 Orsay Cedex, France

E-mail: eanxolab@icmo.u-psud.fr

[b] Current address: Service de Bioénergétique, CNRS URA 2096, Département de Biologie Joliot Curie, CEA Saclay, Bât 532, 91191 Gif-sur-Yvette, France

E-mail: hureau@ozias.saclay.cea.fr

[c] CEA Saclay, DRECAM/SCM Bât 125, 91191 Gif-sur-Yvette, France

Supporting information for this article is available on the WWW under <http://www.eurjic.org> or from the author.

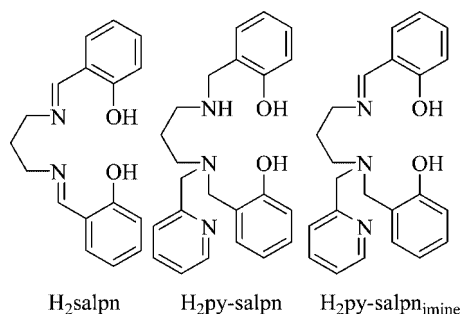
to be attacked by the second water molecule bound to the calcium ion to form the O–O bond.^[13]

The water oxidation mechanisms proposed by Siegbahn et al.^[14–16] and Brudvig et al.^[17] all rely on a tightly bound Ca²⁺ ion located close to a manganese ion. Indeed, it is proposed that during the Kok cycle only one of the Mn ions binds a water substrate molecule and, before dioxygen formation, produces either a highly reactive electrophilic intermediate or an Mn^{IV}-oxyl radical. A Mn^V centre has also been advocated by Pecoraro et al.^[18] In these assumptions, the reactive manganese ion would be the fourth manganese ion of the “3+1” tetranuclear complex.

The large number of papers found in the literature attests that high-valent manganese compounds have been developed as selective organic oxidation catalysts,^[19–25] and tested in bleaching processes.^[26–28] Consequently, generating high-valent and/or Mn-oxo complexes is a relevant challenge for inorganic chemists, both for OEC modelling and for the development of oxidation catalysts.

Among the numerous manganese compounds synthesised, complexes containing Schiff-base ligands, like H₂salen or H₂salpn,^[29] or their derivatives, have been intensively studied as much for their biological relevance^[30–33] as for their catalytic activity.^[25,28,34–38] Indeed, these complexes possess the ability to form high-valent Mn-oxo species,^[39,40] the sixth position being occupied by various ligands.^[41,42] In particular, the use of pyridine as the sixth ligand has been proposed to assist the formation of Mn^V-oxo species from the [(salen)Mn^{III}]⁺ complex, using *tert*-butyl hydroperoxide as the oxidant.^[25]

Taking into account these different elements, we designed a new bulky pentadentate ligand, derived from reduced H₂salpn by the addition of one pyridine arm and denoted H₂py-salpn (see Scheme 1). In the present work, we describe the synthesis and the crystal structure of the new trinuclear manganese complex [(py-salpn)Mn^{III}(μ-OAc)-Mn^{II}(μ-OAc)Mn^{III}(py-salpn)](BPh₄)₂ [**1**(BPh₄)₂]. The magnetic and EPR properties of **1**(BPh₄)₂ have been investigated on crystalline product. Characterisations of complex **1**(BPh₄)₂ upon dissolution in acetonitrile have been performed by EPR and UV/Visible spectroscopy, as well as cyclic voltammetry and mass spectrometry. We also describe the reactivity of **1** upon addition of *tert*-butyl hydroperoxide, where EPR spectroscopy suggests the formation



Scheme 1. H₂salpn, H₂py-salpn and H₂py-salpn_{imine}.

of mononuclear Mn^{IV} species that are identified as Mn^{IV}-OH complexes by mass spectrometry measurements.

Results and Discussion

The reaction of H₂py-salpn with Mn^{III}(OAc)₃·2H₂O in ethanol solution leads to the formation of the cation [(py-salpn)Mn^{III}(μ-OAc)Mn^{II}(μ-OAc)Mn^{III}(py-salpn)]²⁺ (**1**), which was precipitated by addition of two equivalents of sodium tetraphenylborate. It is worth noting that the presence of Mn^{II} in the complex is not unexpected considering that the Mn^{III}(OAc)₃·2H₂O starting material contains Mn^{II} species, even after recrystallisation.

Crystal Structure of [(py-salpn)Mn^{III}(μ-OAc)Mn^{II}(μ-OAc)-Mn^{III}(py-salpn)]²⁺ (**1**)

The structure of complex **1** is presented in Figure 1 and principal bond lengths and angles are listed in Table 1. The cation consists of three manganese ions, two (py-salpn)²⁻

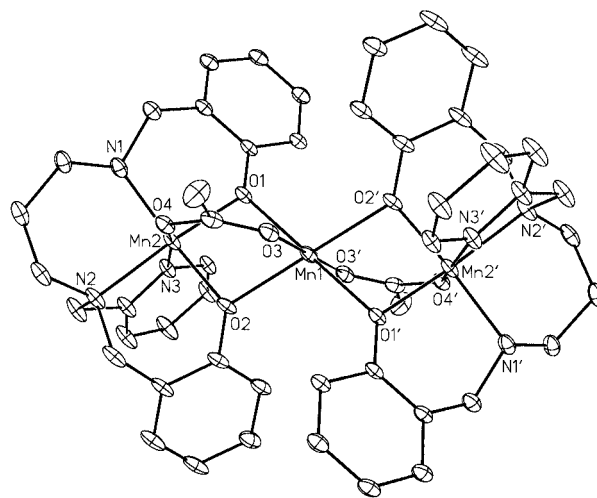


Figure 1. ORTEP view of the cation of **1**, with 10% thermal ellipsoids, showing the atom labelling scheme.

Table 1. Selected bond lengths [Å] and angles [°] for **1**.^[a]

Mn1–O1	2.158(3)	Mn2–O4	2.099(3)
Mn1–O2	2.191(3)	Mn2–N1	2.059(5)
Mn1–O3	2.155(4)	Mn2–N2	2.141(4)
Mn2–O1	1.940(3)	Mn2–N3	2.234(4)
Mn2–O2	1.924(4)	Mn1···Mn2	3.1224(13)
O1–Mn1–O1'	180.0	O2–Mn2–N1	175.86(14)
O2–Mn1–O2'	180.0	O2–Mn2–O4	91.60(14)
O3–Mn1–O3'	180.0	O2–Mn2–N2	92.67(18)
O1–Mn1–O2	72.85(12)	O2–Mn2–N3	86.87(16)
O1–Mn1–O3	86.70(14)	O4–Mn2–N1	88.39(16)
O2–Mn1–O3	86.03(13)	O4–Mn2–N2	91.26(14)
O1–Mn2–N1	91.98(16)	O4–Mn2–N3	169.62(13)
O1–Mn2–O2	83.89(14)	N1–Mn2–N2	91.47(19)
O1–Mn2–O4	93.90(13)	N1–Mn2–N3	93.89(18)
O1–Mn2–N2	173.87(17)	N2–Mn2–N3'	78.57(15)
O1–Mn2–N3	96.14(14)	Mn2···Mn1···Mn2'	180.0

[a] Symmetry transformation used to generate equivalent atoms: $-x, -y, -z + 1$.

ligands and two bridging acetate ions. The Mn1 ion is located at the inversion centre of the cation in a quasi-regular octahedral geometry. The Mn1 and Mn2 (or Mn2') ions are held together by two bridging phenolato arms from one (py-salpn)²⁻ ligand and by one bridging acetate ion. Mn1 is coordinated by the four phenolic bridging oxygen atoms from the two (py-salpn)²⁻ ligands that indeed form a plane and, quasi-perpendicularly to it, by two oxygen atoms from the two acetate bridging ligands. Mn2 and Mn2' are coordinated by the three nitrogen atoms and the two bridging phenolato arms of the (py-salpn)²⁻ ligand and by one oxygen atom from the acetate bridging ligand. The phenolato arms are in a *cis* position, as are two amine nitrogen atoms, whereas the pyridine nitrogen atom and the oxygen atom of the acetate ion are in a *trans* position. The metal–ligand distances reported in Table 1 reveal that **1** is a valence-trapped Mn^{III}Mn^{II}Mn^{III} complex, with the terminal Mn^{III} ions exhibiting a Jahn–Teller elongation along the acetate–Mn–pyridine (O4–Mn2–N3) direction. The bridging acetate ions are in the usual *syn-syn* coordination mode, as reported for analogous trinuclear manganese complexes.^[43] The distance between the Mn^{II} and the Mn^{III} ions in **1** is 3.1224(13) Å, which is slightly shorter than that reported in similar core units (3.137–3.173 Å).^[44] It is, however, significantly shorter than in μ -alkoxo-bis- μ -carboxylato-bridged Mn^{III}Mn^{II}Mn^{III} trinuclear complexes (3.419–3.551 Å).^[45–49] The presence of two phenolato bridges in **1** is the origin of this shortening of the distance. Crystal data also reveal that the secondary amine function is not oxidised during the metallation [N1–C7 = 1.501(7) Å], as could be anticipated from reported syntheses of similar complexes.^[50]

IR, Magnetic and EPR Properties of 1(BPh₄)₂

The IR spectrum of 1(BPh₄)₂ presents significant absorption bands at 1602, 1559, 1424, 760, 734 and 708 cm⁻¹. The three bands detected below 800 cm⁻¹ are assigned to the tetraphenylborate counterions, whereas the two broad bands detected at 1559 and 1424 cm⁻¹ are attributed to the bridging acetate ions.^[51,52] The difference of 135 cm⁻¹ calculated between the symmetrical and the unsymmetrical C=O vibration bands is in agreement with the *syn-syn* bridging coordination mode of the acetate ions.^[51] The C=N vibration band of the pyridine function is detected at 1602 cm⁻¹. Lastly, the absence of a broad absorption band near 1630 cm⁻¹ confirms the absence of the imine function in **1**.^[53]

The product of the molar magnetic susceptibility, χ_M , and the temperature, T , recorded on a powder sample of 1(BPh₄)₂·3CH₃CN is approximately constant between 50 and 300 K. The $\chi_M T$ product lies between 10.31 and 10.37 cm³ mol⁻¹ K. This is close to the theoretical value of 10.375 cm³ mol⁻¹ K expected for two $S_{\text{Mn}^{\text{III}}} = 2$ and one $S_{\text{Mn}^{\text{II}}} = 5/2$ uncoupled spins with g -factor values fixed to 2. The observed temperature dependence indicates that the manganese ions are very weakly coupled. This contrasts

with the μ -alkoxo-bis- μ -carboxylato-Mn^{II}Mn^{III} core complexes that are usually found to be weakly antiferromagnetically coupled, with $J_{\text{Mn}^{\text{II}}\text{Mn}^{\text{III}}}$ lying between -8 and -14.2 cm⁻¹, using the expression $-J S_{\text{Mn}^{\text{II}}} S_{\text{Mn}^{\text{III}}}$ for the exchange Hamiltonian within a pair.^[47–49] A weak exchange interaction, either antiferromagnetic or ferromagnetic, has been observed in analogous Mn^{III}Mn^{II}Mn^{III} trinuclear systems where the Mn^{III} and the Mn^{II} ions are connected by one phenolato, one alkoxo and one carboxylato bridge.^[44] The magnitude of the exchange interaction is indeed controlled by the presence of two alkoxo or phenoxo bridges. Such doubly bridged Mn^{II}Mn^{III} core units present J values ranging from -3.4 to 13.2 cm⁻¹.^[31,54–56]

The X-band EPR spectrum was recorded at 10 K using the conventional perpendicular mode on a powder sample of complex 1(BPh₄)₂·3CH₃CN and is presented in Figure S1 (trace a). An intense and broad line is observed at 335 mT ($g_{\text{eff}} = 2$). Two weaker lines are also detected at 145 and 558 mT, which are strongly indicative of weak interactions between the Mn ions within complex **1**. In the absence of an interaction between the metal ions, the EPR signal would originate solely from the Mn^{II} site as the Jahn–Teller-elongated Mn^{III} centres exhibit a strong zero-field splitting effect that prevents the detection of any EPR signal at 9 GHz. In addition, the regular environment of the Mn^{II} ion should induce a small zero-field splitting effect. Consequently, a broad line at $g_{\text{eff}} = 2$ is expected. The dipolar and isotropic exchange interactions between the central Mn^{II} site and the two terminal Mn^{III} ions split this signal quasi-symmetrically and new lines appear at both lower and higher fields. This was checked by calculating powder X-band EPR spectra for a fictitious system containing two terminal $S = 1$ and one central $S = 1/2$ sites. The profile is, however, strongly dependent on the relative orientation of the terminal zero-field splitting tensors towards that of the dipolar tensors and on the nature – ferro- or antiferromagnetic – of the exchange interaction (see Figure S2 in the Supporting Information). Due to the important spin values of the manganese ions and to the number of parameters, no simulation was attempted on the real system.

Characterisation of 1(BPh₄)₂ upon Dissolution in Acetonitrile

The X-band EPR spectra of millimolar dichloromethane and acetonitrile solutions of complex **1** at 10 K are presented in Figure S1 (see Supporting Information; traces b and c, respectively). The EPR signatures of complex **1** upon dissolution are close to that recorded for a powder sample. In acetonitrile solvent, however, an additional six-line signal is detected at $g_{\text{eff}} = 2$, which is attributed to solvated Mn^{II}. This contribution has been quantified (See Experimental Section for details) and accounts for less than 5% of the total Mn-based species. This experiment shows that the trinuclear structure of complex **1** is essentially maintained upon dissolution in acetonitrile.

The UV/Visible spectrum of complex **1** in acetonitrile is reproduced in Figure 2 (dashed line-left scale). Two major

bands are detected at 587 and 359 nm, with extinction coefficient values (ϵ) of 3.1 and $8.9 \times 10^3 \text{ M}^{-1} \text{ cm}^{-1}$, respectively, with a shoulder at 450 nm ($\epsilon = 4.0 \times 10^3 \text{ M}^{-1} \text{ cm}^{-1}$). The band at 587 nm is attributed to a phenolato \rightarrow Mn^{III} ligand-to-metal charge transfer (LMCT) transition,^[50,53,57,58] whereas the other two transitions may originate from either phenolato \rightarrow Mn^{III} or acetato \rightarrow Mn^{III} LMCT transitions.^[59] The large ϵ values of the LMCT transitions prevent the observation of the Mn^{III} d-d transitions, which are theoretically expected with lower ϵ values.^[60,61]

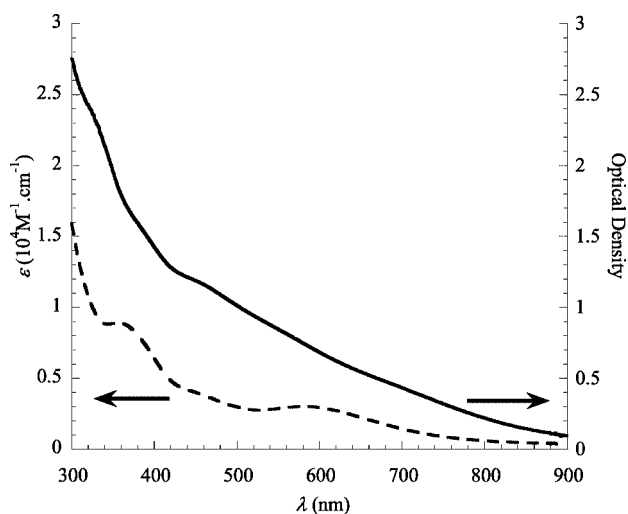


Figure 2. UV/Visible spectra of complex **1**(BPh₄)₂ (10^{-3} M in acetonitrile, dashed line) and immediately after the addition of 20 equivalents of *t*BuOOH (solid line). $T = 20$ °C, $l = 1$ mm.

The cyclic voltammogram recorded under argon on a millimolar solution of complex **1** in acetonitrile in the presence of 0.1 M tetrabutylammonium perchlorate is presented in Figure 3. Two quasi-reversible waves of equal intensity are detected when scanning towards cathodic potentials at $E_{1/2} = 0.140$ ($\Delta E^P = 80$ mV) and -0.075 V vs. SCE ($\Delta E^P = 80$ mV), respectively.^[62] When scanning towards anodic potentials, an intense irreversible wave is observed at $E^P = 0.88$ V vs. SCE that remains irreversible when reversing the scan at 1.0 V vs. SCE. A second, weaker-intensity, irreversible wave is detected at $E^P = 1.16$ V vs. SCE. The two reduction waves are attributed to two successive one-electron reductions of complex **1**, leading firstly to [(py-salpn)-Mn^{III}(μ -OAc)Mn^{II}(μ -OAc)Mn^{II}(py-salpn)]⁺ and then to [(py-salpn)Mn^{II}(μ -OAc)Mn^{II}(μ -OAc)Mn^{II}(py-salpn)]. The Mn^{III}/Mn^{II} reduction process presents low potential values, as it is to be expected considering the anionic environment of the Mn^{III} centre. These values are close to those reported for other diphenolato-coordinated Mn^{III} complexes.^[63] The detection of two single-electron Mn^{III}/Mn^{II} processes presenting $E_{1/2}$ potentials that differs by 225 mV ($\Delta E_{1/2}$) is indicative of a weak electrostatic interaction between the two Mn^{III} ions. The low $\Delta E_{1/2}$ value is related to the long distance between the two Mn^{III} ions (6.24 Å).^[64] The first anodic process detected is attributed to the oxidation of the tetraphenylborate counterion of complex **1**,^[65] and the second irreversible anodic process may be attributed to the oxi-

dation of complex **1**, leading to the formation of [(py-salpn)-Mn(μ -OAc)Mn(μ -OAc)Mn(py-salpn)]³⁺, which further evolves chemically. Unfortunately, the interaction of the oxidised tetraphenylborate ion generated at the electrode surface with complex **1** and/or with the [(py-salpn)Mn(μ -OAc)Mn(μ -OAc)Mn(py-salpn)]³⁺ species renders the process difficult to analyse.

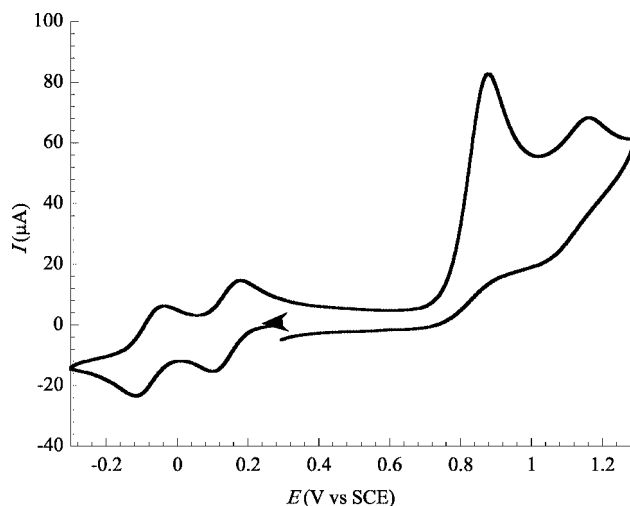


Figure 3. Cyclic voltammograms of **1**(BPh₄)₂ (10^{-3} M in acetonitrile with 0.1 M of tetrabutylammonium perchlorate). $T = 20$ °C and scan rate = 100 mV s^{-1} .

Chemical Oxidation

The chemical oxidation of complex **1** was performed on a millimolar acetonitrile solution with *tert*-butyl hydroperoxide (*t*BuOOH) as the oxidant. The oxidant was added in large excess (20 equivalents). Upon addition, the solution turned from dark green to black. We will show in the next

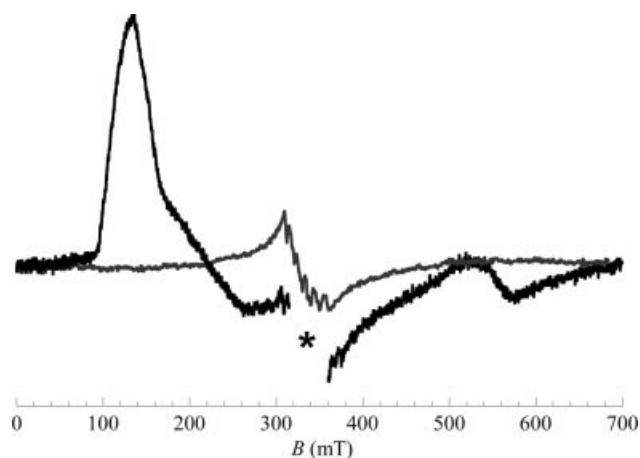


Figure 4. EPR spectra of complex **1**(BPh₄)₂ (10^{-3} M in acetonitrile, grey line) and immediately after the addition of 20 equivalents of *t*BuOOH (black line). Recording conditions: 0.5 mT modulation amplitude, 100 kHz modulation frequency, $T = 100$ K, 2.0 mW microwave power, $\nu = 9.39$ GHz. The *t*BuO[•] radical signal has been removed off the black trace.

section that the chemical oxidation of complex **1** leads to the formation of high-valent Mn species (**1ox**). The **1ox** species were characterised by UV/Visible and EPR spectroscopy and ESI mass spectrometry.

The UV/Visible spectrum of **1ox**, shown in Figure 2 (solid line, right scale), is mainly featureless in the visible re-

gion and presents a strong absorbance in the UV domain. Shoulders are observed at 463 and 685 nm. These observations are reminiscent of previous observations for hydroxyl-rich^[66] or for carboxylato^[67] mononuclear Mn^{IV} Schiff-base complexes. The intense absorption band in the UV region may therefore be attributed to a phenolato→Mn^{IV} or to a

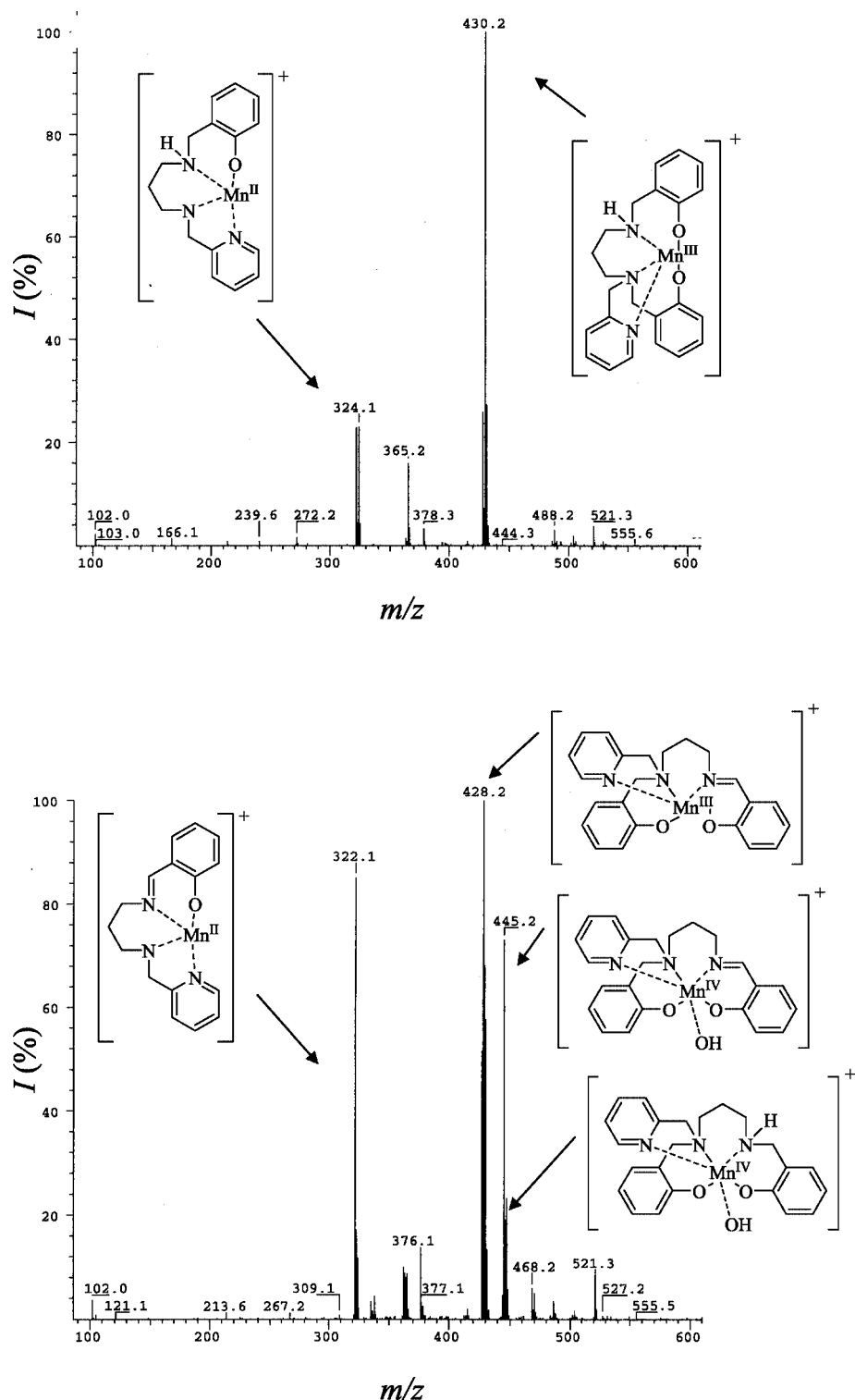


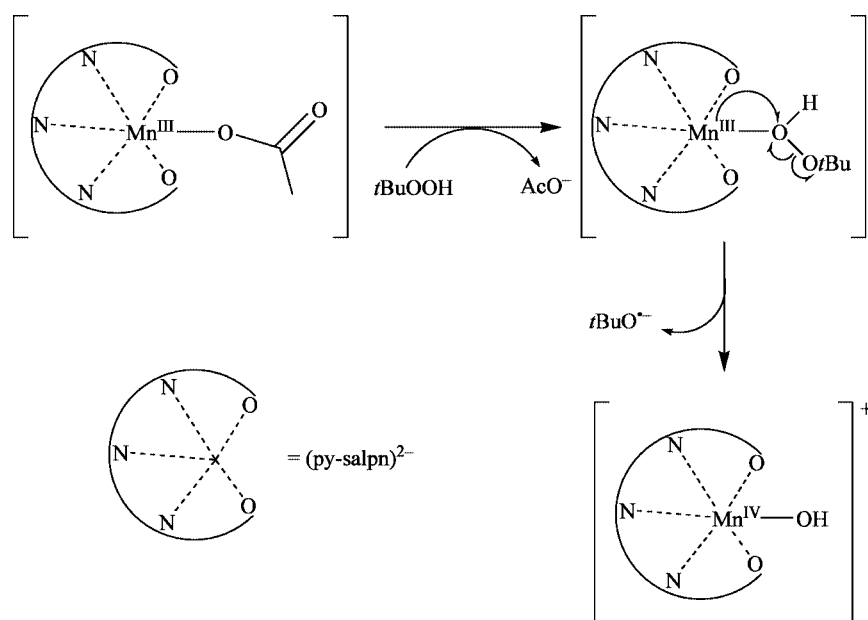
Figure 5. Electrospray mass spectrum of complex **1** (10⁻⁴ M in acetonitrile) recorded for the starting solution (top) and after addition of 20 equivalents of *t*BuOOH (bottom).

hydroxo→Mn^{IV} LMCT transition. The shoulders observed in the visible region can be attributed to a poorly resolved phenolato→Mn^{IV} MLCT^[50,53,57] or to Mn^{IV} d-d transitions, the strong intensity of which originates from the tail of the absorption in the UV region.

The X-band EPR spectrum of **1ox** at 100 K, recorded in the perpendicular detection mode, is presented in Figure 4 (black line). An intense $g = 2$ signal corresponding to an organic radical has been removed for clarity. The EPR signature of complex **1** recorded under the same conditions is also reproduced (grey line in Figure 4). The signal of complex **1** differs slightly from trace c of Figure S2, with the low-field transitions being undetectable at this recording temperature. Four new transitions appear at $g_{\text{eff}} = 4.9, 3.0, 1.5$ and 1.17 after the addition of the oxidant.^[68] These resonances are broad and show no evidence for ⁵⁵Mn hyperfine coupling. The EPR signature of **1ox** is indicative of an $S = 3/2$ Mn^{IV} ion. The complexity of the EPR spectrum of a d³ species depends on the magnitude of the zero-field splitting (ZFS) compared to the applied microwave frequency. In axial symmetry ($E/D = 0$), two limiting cases can be discussed depending on the relative magnitude of $|2D|$ vs. $h\nu$, where D is the axial ZFS parameter. At X-band ($h\nu = 0.3 \text{ cm}^{-1}$), and when $|2D| \gg h\nu$, the ZFS effect dominates the Zeeman effect, and a strong transition is expected at low field ($g_{\text{eff}} \approx 4$) with a weak component at around $g_{\text{eff}} = 2$. This behaviour has been observed for numerous Mn^{IV} centres with anionic chelating ligands, such as hydroxo, phenolato, carboxylato or anilido.^[57,66,67,69–74] When $|2D| \ll h\nu$, the Zeeman effect dominates the ZFS effect and the signal is centred at $g_{\text{eff}} \approx 2$, with weaker lines at both the low- and high-field edges. This behaviour has been reported for rare Mn^{IV}-tetraphenolato,^[72] Mn^{IV}-thiohydroxamato,^[75] and Mn^{IV}-thiocarbamato^[76] complexes. The strong absorption detected at $g_{\text{eff}} = 4.9$ and the weaker one

near $g_{\text{eff}} = 1.5$ suggest that the present Mn^{IV} species exhibits a strong ZFS effect. The divergence from a g_{eff} value of around 4 originates from the rhombicity of the ZFS. According to the diagram showing the evolution of the g_{eff} values for the two Kramer doublets as a function of E/D ,^[77] one can see that the line positions at $g_{\text{eff}} = 4.9, 3.0, 1.5$ and 1.17 can be well reproduced with $E/D = 0.17$. These first two characterisations suggest that **1ox** is a mononuclear Mn^{IV} species.

In order to identify the Mn^{IV} species formed, ESI/MS experiments were performed. The mass spectra of complexes **1** and **1ox** are presented in Figure 5. The mass spectrum of complex **1** exhibits a major molecular peak at $m/z = 430$ amu and three other peaks at $m/z = 322, 324$ and 365 amu.^[78] The first peak is attributed to the mononuclear Mn^{III} entity $\{[(\text{py-salpn})\text{Mn}]\}^+$, and the peaks at 322 and 324 amu correspond to Mn^{II} species, namely $\{[(\text{L}^1_{\text{imine}})\text{Mn}]\}^+$ and $\{[(\text{L}^1)\text{Mn}]\}^+$, where L¹ stands for the (py-salpn)²⁻ ligand after the loss of one phenolato arm and L¹_{imine} for L¹ with a reduced secondary amine function (see Figure 5). The peak at $m/z = 365$ amu can be attributed to the adduct $\{[(\text{L}^1)\text{Mn}]\text{CH}_3\text{CN}\}^+$, even though such solvated species are rarely detected under the present recording conditions. After addition of *t*BuOOH, the peak at $m/z = 430$ amu disappears and the peak at 322 amu increases in intensity together with the apparition of three new peaks at $m/z = 428, 445$ and 447 amu. The peak at 428 amu corresponds to the Mn^{III} species $\{[(\text{py-salpn}_{\text{imine}})\text{Mn}]\}^+$, where subscript imine means that the secondary amine function has been oxidised to an imine (Scheme 1). The peaks at 445 and 447 are attributed to the mononuclear hydroxo Mn^{IV} entities $\{[(\text{py-salpn}_{\text{imine}})\text{Mn}(\text{OH})]\}^+$ and $\{[(\text{py-salpn})\text{Mn}(\text{OH})]\}^+$, respectively. It is worth noting that the formation of the imine function may be due to the use of the oxidant *t*BuOOH. Species **1ox** is subsequently attributed to



Scheme 2. Proposed mechanism for the formation of the Mn^{IV}-OH species.

the mixture of the two Mn^{IV} monocations $\{[(\text{py-salpn}_{\text{imine}})\text{Mn}(\text{OH})]\}^+$ and $\{[(\text{py-salpn})\text{Mn}(\text{OH})]\}^+$.

Lastly, according to the EPR spectra, we can propose that the central Mn^{II} ion is oxidised into an EPR-silent Mn^{III} species, the UV/Visible signature of which may be masked by the tail of the UV absorbance of complexes **1ox**.

Formation of the Mn^{IV}-hydroxo Entities

A mechanism for the formation of the Mn^{IV}-hydroxo species **1ox** is tentatively proposed in Scheme 2. For clarity, only the terminal Mn^{III} ions of complex **1** are considered. We propose that after the coordination of the *t*BuOOH oxidant to the Mn^{III} centre, the homolytic breakage of the O–O bond^[79] would lead to the release of the radical *t*BuO[•] and to the formation of the Mn^{IV}–OH complex.

We should mention that it is also plausible that the acetate ion, which is a particularly strong base in acetonitrile ($\text{p}K_{\text{a}} = 22$)^[80] would be able to deprotonate the hydroxo ion coordinated to the Mn^{IV} ion, thus forming a Mn^{IV}–oxo species. The EPR and UV/Visible spectra do not allow us to discriminate an oxo from a hydroxo Mn^{IV} species. The detection in of peaks at 445 and 447 amu in the ESI mass spectrum may then be explained by the formation of a proton adduct of the neutral Mn^{IV}–oxo entities, leading to $\{[(\text{py-salpn}_{\text{imine}})\text{Mn}(\text{O})\text{H}]\}^+$ and $\{[(\text{py-salpn})\text{Mn}(\text{O})\text{H}]\}^+$. It is also worth noting that the presence of the oxidised ligand may be due to the formation of Mn^{IV} species or to the *t*BuOOH itself.

Concluding Remarks

A new trinuclear Mn^{III}Mn^{II}Mn^{III} complex **1** containing a bulky [N₃O₂] ligand derived from the H₂salpn Schiff-base ligand by the addition of one pyridine arm has been isolated and X-ray characterised. This complex has been fully characterised by magnetic studies, UV/Visible, IR and EPR spectroscopy, cyclic voltammetry and ESI mass spectrometry. The chemical oxidation of the trinuclear complex **1** by *t*BuOOH leads to the formation of Mn^{IV} entities, which are UV/Visible and EPR characterised and identified by mass spectrometry as mononuclear Mn^{IV}–OH species.

From the recent crystallographic data obtained for the *Synechococcus elongatus* PSII, a “3+1” structure has been proposed for the OEC. Some water oxidation mechanisms consistent with this recent structure favour the role of a unique highly reactive Mn ion. In this context, the synthesis and the complete characterisation of trinuclear species as well as high-valence mononuclear Mn entities remains highly relevant for the spectroscopic OEC modelling. In the near future, it will be interesting to substitute the central Mn^{II} ion in complex **1** by a calcium ion as such a putative complex should present some OEC relevant Mn–Ca–carboxylate interactions.

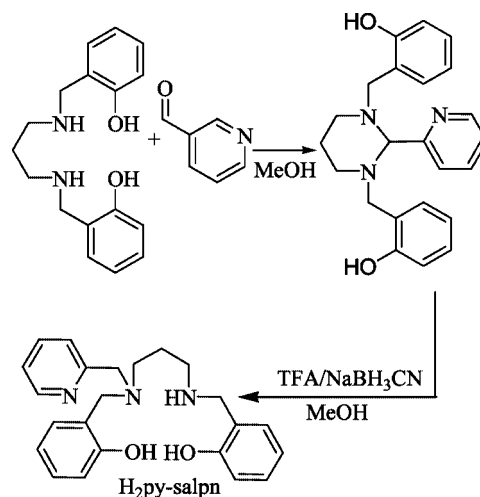
Experimental Section

General Remarks: Reagents and solvents were purchased commercially and used as received. Elemental Analysis was performed by

the Service de Microanalyse of the CNRS (Gif sur Yvette, France) for carbon, nitrogen and hydrogen and by the Service Central d'Analyse of CNRS (Vernaison, France) for manganese and chloride. Infrared spectra were recorded as KBr pellets in the range of 4000 to 200 cm⁻¹ with a Perkin–Elmer Spectrum 1000 spectrophotometer. ¹H NMR spectra were recorded with a Bruker AM-250 (250 MHz) spectrometer. Electrospray ionisation mass spectra were recorded with a Finnigan Mat95S in a BE configuration at low resolution on millimolar acetonitrile solutions.

Caution: Perchlorate salts of metal complexes with organic ligands are potentially explosive. Only small quantities of these compounds should be prepared and they should be handled behind suitable protective shields.

Synthesis of H₂py-salpn: The two-step synthesis of the ligand H₂py-salpn from the reduced H₂salpn is shown in Scheme 3. The reduced H₂salpn ligand 2.86 g, (10 mmol), prepared according to a previously reported synthesis,^[57] was dissolved in 100 mL of methanol and 2-pyridinecarboxaldehyde (1 mL, 10 mmol) was added with stirring. The white precipitate that appeared was filtered and washed with methanol, and then redissolved in methanol by addition of two equivalents of trifluoroacetic acid. Two equivalents of sodium cyanoborohydride were added and the solution was stirred for 12 h. Methanol was eliminated and 150 mL of water was added. The aqueous solution was extracted three times with 50 mL of dichloromethane. After removal of the solvent, H₂py-salpn was obtained as a yellow oil. Yield: 62% (2.3 g). ¹H NMR (250 MHz, CDCl₃): $\delta = 8.29$ (d, $J = 4.6$ Hz, 1 H, *H*-Py), 7.62–7.55 (m, 2 H, *H*-Ar), 7.18–7.05 (m, 3 H, *H*-Ar), 7.00–6.93 (m, 2 H, *H*-Ar), 6.86 (d, 1 H, *H*-PhOH), 6.79 (d, 1 H, *H*-PhOH), 6.72–6.65 (m, 2 H, *H*-Ar), 3.91 (s, 2 H, RN-CH₂-PhOH), 3.77 (s, 2 H, RN-CH₂-Py), 3.54 (s, 2 H, HN-CH₂-PhOH), 2.65 (t, $J = 5.8$ Hz, 2 H, HN-CH₂-CH₂), 2.55 (t, $J = 5.8$ Hz, 2 H, RN-CH₂-CH₂), 1.78 (q, $J = 5.8$ Hz, 2 H, CH₂-CH₂-CH₂) ppm. ¹³C NMR (62.9 MHz, CDCl₃) 157.5, 157.3, 156.6, 148.7, 137.3, 130.5, 129.8, 129.5, 129.3, 123.4, 122.9, 122.5, 120.0, 119.2, 119.1, 116.6, 58.2, 56.7, 52.2, 51.0, 47.6, 24.4 ppm. IR: $\tilde{\nu} = 1674$ cm⁻¹ (s), 1613 (m), 1595 (s), 1489 (m), 1460 (s), 1436 (m), 1383 (m), 1265 (s), 1201 (m), 1134 (m), 1104 (w), 737 (s). ESI-MS: m/z (%) = 378.2 (45) [M + H]⁺, 272.2 (100) [M – CH₂PhOH + H]⁺, 166.1 (60) [M – 2CH₂PhOH + H]⁺.



Scheme 3. Synthetic route from reduced H₂salpn to H₂py-salpn.

Synthesis of [(py-salpn)Mn^{III}(μ -OAc)Mn^{II}(μ -OAc)Mn^{III}(py-salpn)]-(BPh₄)₂·2CH₃CN·0.5H₂O [1** (BPh₄)₂·2CH₃CN·0.5H₂O]:** Mn(OAc)₃·2H₂O (268 mg, 1.0 mmol) was added to a 5 mL ethanol solution

of H₂py-salpn (377 mg, 1.0 mmol). The solution turned from purple to dark green. Addition of an excess (1.5 mmol) of sodium tetraphenylborate led to the precipitation of a dark green powder, which was collected by filtration and washed carefully with ethanol. Yield: 68% (239 mg). C₁₀₂H₁₀₃B₂N₈O_{8.5}Mn₃ [1(BPh₄)₂·2CH₃CN·0.5H₂O] (1761): calcd. C 69.5, H 5.9, N 6.3, B 1.2, Mn 9.3; found C 69.3, H 5.7, B 1.2, Mn 9.4, N 6.2. IR: $\tilde{\nu}$ = 3439 cm⁻¹ (m), 3176 (m), 3054 (m), 1602 (m), 1558 (s), 1483 (s), 1458 (m), 1444 (m), 1425 (s), 1345 (w), 1249 (s), 1204 (w), 1113 (w), 1006 (w), 791 (w), 760 (m), 734 (m), 708 (m), 655 (w), 612 (m), 573 (w). The powder was then redissolved in acetonitrile and the solution was filtered and placed in an atmosphere of diethyl ether. Crystals of 1(BPh₄)₂·3CH₃CN suitable for X-ray crystallographic study were obtained, collected by filtration, washed with diethyl ether and dried in air.

Crystallographic Data Collection and Refinement of the Structure of 1(BPh₄)₂·3CH₃CN: The crystal data of 1(BPh₄)₂·3CH₃CN and the parameters of data collection are summarised in Table 2. Crystal data for 1(BPh₄)₂·3CH₃CN were collected on a Nonius Kappa-CCD area detector diffractometer using graphite-monochromated Mo-K α radiation. The lattice parameters were determined from ten images recorded with 2° φ -scans and later refined on all data. The data were recorded at 123 K. A 180° φ -range was scanned with 2° steps with a crystal-to-detector distance fixed at 30 mm. Data were corrected for Lorentz polarisation. The structures were solved by direct methods with SHELXS-86^[81] and refined by full-matrix least-squares on F^2 with anisotropic thermal parameters for all non-H atoms with SHELXTL-93^[82] H atoms (unless H of CH₃CN solvent molecule) were introduced at calculated positions as riding atoms with an isotropic displacement parameter equal to 1.2 (CH, and CH₂) or 1.5 (CH₃) times that of the parent atom. The CH₃CN solvent molecules were found disordered over two positions with 0.5 occupancy factors. The molecular plots were drawn with

Table 2. Details of structure determination, refinement and experimental parameters for 1(BPh₄)₂·3CH₃CN.

Empirical formula	C ₁₀₄ H ₁₀₃ B ₂ Mn ₃ N ₉ O ₈
Formula mass [g mol ⁻¹]	1793.39
Temperature [K]	123(2)
Wavelength [Å]	0.71073
Crystal system	triclinic
Space group	$P\bar{1}$
<i>a</i> [Å]	11.573(2)
<i>b</i> [Å]	14.073(3)
<i>c</i> [Å]	15.889(3)
α [°]	71.26(3)
β [°]	85.08(3)
γ [°]	72.05(3)
Volume [Å ³]	2331.0(9)
<i>Z</i>	1
Density (calculated) [g cm ⁻³]	1.278
Absorption coefficient [mm ⁻¹]	0.462
Crystal size [mm]	0.15 × 0.10 × 0.10
θ range for data collection [°]	2.47 to 24.70
Index ranges	0 ≤ <i>h</i> ≤ 13, -15 ≤ <i>k</i> ≤ 16, -18 ≤ <i>l</i> ≤ 18
Reflections collected	14334
Independent reflections/ <i>R</i> (int)	7285 [<i>R</i> (int) = 0.0530]
Data	4705
Parameters	601
Goodness-of-fit on F^2	0.913
Final <i>R</i> indices [<i>I</i> > 2 σ (<i>I</i>)]	<i>R</i> ₁ = 0.0704, <i>wR</i> ₂ = 0.1893
<i>R</i> indices (all data)	<i>R</i> ₁ = 0.1131, <i>wR</i> ₂ = 0.2265
Largest diff. peak/hole [e Å ⁻³]	0.631/-0.433

SHELXTL.^[83] All calculations were performed on a Silicon Graphics R10000 workstation.

CCDC-233590 contains the supplementary crystallographic data for this paper. These data can be obtained free of charge from The Cambridge Crystallographic Data Centre via www.ccdc.cam.ac.uk/data_request/cif.

Magnetic Susceptibility Measurements: Magnetic susceptibility data were recorded on a MPMS5 magnetometer (Quantum Design Inc.). The calibration was made at 298 K using a palladium reference sample furnished by Quantum Design Inc. The data were collected over a temperature range of 50–300 K at a magnetic field of 5000 Oe and were corrected for diamagnetism.

EPR Spectroscopy: EPR spectra were recorded with a Bruker ELEXSYS 500 spectrometer at X-band. For low-temperature studies, an Oxford Instruments continuous flow liquid helium cryostat and a temperature control system were used. The quantity of free Mn^{II} was estimated by comparison with spectra of Mn(ClO₄)₂·6H₂O dissolved in acetonitrile to various concentrations.

Cyclic Voltammetry: Cyclic voltammetry measurements were recorded with an EGG PAR potentiostat (M273 model). The counter electrode was an Au wire, the working electrode a glassy carbon disk, which was carefully polished before each voltammogram with a 1- μ m diamond paste, sonicated in an ethanol bath and then washed carefully with ethanol. The reference electrode was an Ag/AgClO₄ electrode (0.530 V vs. NHE electrode), isolated in a fritted bridge. The solvent used was distilled acetonitrile and tetrabutylammonium perchlorate was added to obtain a 0.1 M supporting electrolyte.

UV/Visible Spectroscopy: UV/Visible spectra were recorded with a Cary 300 Bio spectrophotometer at 20 °C with 0.1-cm quartz cuvettes.

Supporting Information (see footnote on the first page of this article): The X-band 10 K EPR spectra of millimolar dichloromethane and acetonitrile solutions of complex 1 are presented in Figure S1 (traces b and c, respectively). Theoretical powder X-band EPR spectra calculated for a trinuclear system with two terminal *S*₁₁ = *S*₁₂ = 1 and one central *S*_c = 1/2 spins (ν = 9.39 GHz, *T* = 10 K) is given in Figure S2.

Acknowledgments

We are grateful to Félix Perez for mass spectrometry measurements, to Guillaume Blain for EPR technical assistance, and to Dr. Alain Boussac (Service de Bioénergétique, URA CNRS 2096, CEA Saclay, Gif-sur-Yvette, France) for EPR facilities. Laurent Sabater is acknowledged for NMR technical assistance. We thank Prof. Jean-Jacques Girerd and Prof. Vincent L. Pecoraro for stimulating discussions. The Conseil Régional de l'Île de France is acknowledged for its contribution to the acquisition of the Bruker ELEXSYS X-band EPR spectrometer. The COST D21 European action and the LRC-CEA project are acknowledged for their financial support.

- [1] E. J. Larson, V. L. Pecoraro, in *Manganese Redox Enzymes* (Ed.: V. L. Pecoraro), VCH Publishers, Inc., New York, **1992**, pp. 1–28.
- [2] J. D. Crowley, D. A. Traynor, D. C. Weatherburn, in *Metal Ions in Biological Processes* (Eds.: A. Sigel, H. Sigel), Marcel Dekker, Basel, Switzerland, **2000**, pp. 209–278.
- [3] R. H. Holm, P. Kennepohl, E. I. Solomon, *Chem. Rev.* **1996**, *96*, 2239–2314.

- [4] V. V. Barynin, M. M. Whittaker, S. V. Antonyuk, V. S. Lamzin, P. M. Harrison, P. J. Artymiuk, J. W. Whittaker, *Structure* **2001**, 9, 725–738.
- [5] V. K. Yachandra, K. Sauer, M. P. Klein, *Chem. Rev.* **1996**, 96, 2927–2950.
- [6] A. W. Rutherford, P. Faller, *Trends Biochem. Sci.* **2001**, 26, 341–344.
- [7] V. K. Yachandra, *Philos. Trans. R. Soc. London, Ser. B* **2002**, 357, 1347–1358.
- [8] A. W. Rutherford, A. Boussac, *Science* **2004**, 303, 1782–1784.
- [9] P. Joliot, G. Barbieri, R. Chabaud, *Photochem. Photobiol.* **1969**, 10, 309–329.
- [10] B. Kok, B. Forbush, M. McGloin, *Photochem. Photobiol.* **1970**, 11, 457–475.
- [11] K. N. Ferreira, T. M. Iverson, K. Maghlaoui, J. Barber, S. Iwata, *Science* **2004**, 303, 1831–1838.
- [12] J. Biesiadka, B. Loll, J. Kern, K.-D. Irrgang, A. Zouni, *Phys. Chem. Chem. Phys.* **2004**, 6, 4733–4736.
- [13] J. P. McEvoy, G. W. Brudvig, *Phys. Chem. Chem. Phys.* **2004**, 6, 4754–4763.
- [14] P. E. M. Siegbahn, R. H. Crabtree, *J. Am. Chem. Soc.* **1999**, 121, 117–127.
- [15] P. E. M. Siegbahn, *Inorg. Chem.* **2000**, 39, 2923–2935.
- [16] P. E. M. Siegbahn, *Curr. Opin. Chem. Biol.* **2002**, 6, 227–235.
- [17] J. S. Vrettos, J. Limburg, G. W. Brudvig, *Biochim. Biophys. Acta* **2001**, 1503, 229–245.
- [18] V. L. Pecoraro, M. J. Baldwin, M. T. Caudle, W.-Y. Hsieh, N. A. Law, *Pure Appl. Chem.* **1998**, 70, 925–929.
- [19] E. M. McGarrigle, D. G. Gilheany, *Chem. Rev.* **2005**, 105, 1563–1602.
- [20] V. C. Quee-Smith, L. DelPizzo, S. H. Jureller, J. L. Kerschner, R. Hage, *Inorg. Chem.* **1996**, 35, 6461–6465.
- [21] D. De Vos, T. Bein, *Chem. Commun.* **1996**, 917–918.
- [22] A. Berkessel, C. A. Sklorz, *Tetrahedron Lett.* **1999**, 40, 7965–7968.
- [23] J. Brinksma, L. Schmieder, G. Van Vliet, R. Boaron, R. Hage, D. E. De Vos, P. L. Alsters, B. L. Feringa, *Tetrahedron Lett.* **2002**, 43, 2619–2622.
- [24] C. Zondervan, R. Hage, B. L. Feringa, *Chem. Commun.* **1997**, 419–420.
- [25] K. Srinivasan, P. Michaud, J. K. Kochi, *J. Am. Chem. Soc.* **1986**, 108, 2309–2320.
- [26] R. Hage, J. E. Iburg, J. Kerschner, J. H. Koek, E. L. M. Lempers, R. J. Martens, U. S. Racherla, S. W. Russell, T. Swarthoff, M. R. P. van Vliet, J. B. Warnaar, L. van der Wolf, B. Krijnen, *Nature* **1994**, 369, 637–639.
- [27] T. Tzedakis, Y. Benzada, M. Comtat, *Ind. Eng. Chem. Res.* **2001**, 40, 3435–3444.
- [28] W. Zhang, J. L. Loebach, S. R. Wilson, E. N. Jacobsen, *J. Am. Chem. Soc.* **1990**, 112, 2801–2803.
- [29] H₂salen = *N,N'*-bis(salicylidene)ethane-1,2-diamine, H₂salpn = *N,N'*-bis(salicylidene)propane-1,3-diamine, H₂py-salpn = *N*-(2-pyridylmethyl)-*N,N'*-bis(2-hydroxybenzyl)propane-1,3-diamine.
- [30] A. J. Wu, J. E. Penner-Hahn, V. L. Pecoraro, *Chem. Rev.* **2004**, 104, 903–938.
- [31] A. Gelasco, M. L. Kirk, J. W. Kampf, V. L. Pecoraro, *Inorg. Chem.* **1997**, 36, 1829–1837.
- [32] M. J. Baldwin, V. L. Pecoraro, *J. Am. Chem. Soc.* **1996**, 118, 11325–11326.
- [33] N. Aurangzeb, C. E. Hulme, C. A. McAuliffe, R. G. Pritchard, M. Watkinson, M. R. Bermejo, A. Garcia-Deibe, M. Rey, J. Sanmartin, A. Sousa, *J. Chem. Soc., Chem. Commun.* **1994**, 1153–1155.
- [34] A. Gelasco, S. Bensiak, V. L. Pecoraro, *Inorg. Chem.* **1998**, 28, 3301–3309.
- [35] F. M. MacDonnell, N. L. P. Flacker, C. Stern, T. V. O'Halloran, *J. Am. Chem. Soc.* **1994**, 116, 7431–7432.
- [36] E. J. Larson, V. L. Pecoraro, *J. Am. Chem. Soc.* **1991**, 113, 7809–7810.
- [37] T. J. Collins, R. D. Powell, C. Slebodnick, E. S. Uffelman, *J. Am. Chem. Soc.* **1990**, 112, 899–901.
- [38] T. J. Collins, S. W. Gordon-Wylie, *J. Am. Chem. Soc.* **1989**, 111, 4511–4513.
- [39] D. Feichtinger, D. A. Plattner, *Chem. Eur. J.* **2001**, 7, 591–599.
- [40] D. Feichtinger, D. A. Plattner, *Angew. Chem. Int. Ed. Engl.* **1997**, 36, 1718–1719.
- [41] J. El-Bahraoui, O. Wiest, D. Feichtinger, D. A. Plattner, *Angew. Chem. Int. Ed.* **2001**, 40, 2073–2076.
- [42] D. Feichtinger, D. A. Plattner, *J. Chem. Soc., Perkin Trans. 2* **2000**, 1023–1028.
- [43] M. Hirotsu, M. Kojima, W. Mori, Y. Yoshikawa, *Bull. Chem. Soc. Jpn.* **1998**, 71, 2873–2884.
- [44] M. Hirotsu, M. Kojima, Y. Yoshikawa, *Bull. Chem. Soc. Jpn.* **1997**, 70, 649–657.
- [45] X. Li, D. P. Kessissoglou, M. L. Kirk, C. J. Bender, V. L. Pecoraro, *Inorg. Chem.* **1988**, 27, 1–3.
- [46] D. P. Kessissoglou, M. L. Kirk, C. A. Bender, M. S. Lah, V. L. Pecoraro, *J. Chem. Soc., Chem. Commun.* **1989**, 84–86.
- [47] D. P. Kessissoglou, M. L. Kirk, M. S. Lah, X. Li, C. Raptopoulou, W. E. Hatfield, V. L. Pecoraro, *Inorg. Chem.* **1992**, 31, 5424–5432.
- [48] V. Tangoulis, D. A. Malamataris, K. Soulti, V. Stergiou, C. P. Raptopoulou, A. Terzis, T. A. Kabanos, D. P. Kessissoglou, *Inorg. Chem.* **1996**, 35, 4974–4983.
- [49] V. Tangoulis, D. A. Malamataris, G. A. Spyroulias, C. P. Raptopoulou, A. Terzis, D. P. Kessissoglou, *Inorg. Chem.* **2000**, 39, 2621–2630.
- [50] C. Hureau, L. Sabater, E. Anxolabéhère-Mallart, M. Nierlich, M.-F. Charlot, F. Gonnet, E. Rivière, G. Blondin, *Chem. Eur. J.* **2004**, 10, 1998–2010.
- [51] S. Pal, J. W. Gohdes, W. C. A. Wilisch, W. H. Armstrong, *Inorg. Chem.* **1992**, 31, 713–716.
- [52] K. Wieghardt, U. Bossek, L. Zsolnai, G. Huttner, G. Blondin, J.-J. Girerd, F. Babonneau, *J. Chem. Soc., Chem. Commun.* **1987**, 651–653.
- [53] O. Horner, E. Anxolabéhère-Mallart, M.-F. Charlot, L. Tchertanov, J. Guilhem, T. A. Mattioli, A. Boussac, J.-J. Girerd, *Inorg. Chem.* **1999**, 38, 1222–1232.
- [54] J. Yoo, A. Yamaguchi, M. Nakano, J. Krzystek, W. E. Streib, L.-C. Brunel, H. Ishimoto, G. Christou, D. N. Hendrickson, *Inorg. Chem.* **2001**, 40, 4604–4616.
- [55] A. Yoshino, T. Miyagi, E. Asato, M. Mikuriya, Y. Sakata, K.-i. Sugiura, K. Iwasaki, S. Hino, *Chem. Commun.* **2000**, 1475–1476.
- [56] H. Diril, H.-R. Chang, X. Zhang, S. K. Larsen, J. A. Potenza, C. G. Pierpont, H. J. Schugar, S. S. Isied, D. N. Hendrickson, *J. Am. Chem. Soc.* **1987**, 109, 6207–6208.
- [57] A. Neves, S. M. D. Erthal, I. Vencato, A. S. Ceccato, Y. P. Mascarenhas, O. R. Nascimento, M. Hörner, A. A. Batista, *Inorg. Chem.* **1992**, 31, 4749–4755.
- [58] J. A. Bonadies, M. J. Maroney, V. L. Pecoraro, *Inorg. Chem.* **1989**, 28, 2044–2051.
- [59] C. Hureau, E. Anxolabéhère-Mallart, M. Nierlich, F. Gonnet, E. Rivière, G. Blondin, *Eur. J. Inorg. Chem.* **2002**, 2710–2719.
- [60] T. S. Davis, J. P. Fackler, M. J. Weeks, *Inorg. Chem.* **1968**, 7, 1994–2002.
- [61] R. Dingle, *Acta Chem. Scand.* **1966**, 20, 33–44.
- [62] $E_{1/2}$ is defined as $(E_a^P + E_c^P)/2$ and $\Delta E^P = |E_a^P - E_c^P|$, where E_a^P (E_c^P) is defined as the potential of the maximum of current intensity when scanning toward anodic (cathodic) potentials.
- [63] See ref.^[57] and references cited therein.
- [64] J.-J. Girerd, E. Anxolabéhère-Mallart, in *Spectroscopic Methods in Bioinorganic Chemistry, Vol. 14* (Eds.: E. I. Solomon, K. O. Hodgson), American Chemical Society, Washington DC, **1998**, pp. 262–271.
- [65] P. K. Pal, S. Chowdhury, M. G. B. Drew, D. Datta, *New J. Chem.* **2002**, 26, 367–371.
- [66] D. P. Kessissoglou, X. Li, W. M. Butler, V. L. Pecoraro, *Inorg. Chem.* **1987**, 26, 2487–2492 and references cited therein.

- [67] S. K. Chandra, P. Basu, D. Ray, S. Pal, A. Chakravorty, *Inorg. Chem.* **1990**, *29*, 2423–2428.
- [68] In addition, a multiline signal of small intensity is detected between 300 and 380 mT. This signal is attributed to the presence of a small quantity of solvated Mn^{II} in solution.
- [69] D. T. Richens, D. T. Sawyer, *J. Am. Chem. Soc.* **1979**, *101*, 3681–3683.
- [70] S. M. Saadeh, M. S. Lah, V. L. Pecoraro, *Inorg. Chem.* **1991**, *30*, 8–15.
- [71] O. Schlager, K. Wieghardt, B. Nuber, *Inorg. Chem.* **1995**, *34*, 6456–6462.
- [72] T. M. Rajendiran, J. W. Kampf, V. L. Pecoraro, *Inorg. Chim. Acta* **2002**, *339*, 497–502.
- [73] T. K. Paine, T. Weyhermüller, E. Bothe, K. Wieghardt, P. Chaudhuri, *Dalton Trans.* **2003**, 3136–3144.
- [74] W. Adam, C. Mock-Knoblauch, C. R. Saha-Möller, M. Herd-erich, *J. Am. Chem. Soc.* **2000**, *122*, 9685–9691.
- [75] S. Pal, P. Ghosh, A. Chakravorty, *Inorg. Chem.* **1985**, *24*, 3704–3706.
- [76] K. L. Brown, R. M. Golding, P. C. Healy, J. K. Jessop, W. C. Tennant, *Aust. J. Chem.* **1974**, *27*, 2075–2081.
- [77] B. H. Huynh, T. A. Kent, in *Advances in Mössbauer Spectroscopy. Applications to Physics, Chemistry and Biology* (Eds.: B. V. Thosar, P. K. Iyengar, J. K. Srivastava, S. C. Bhargava), Elsevier Science Publishers B. V., Amsterdam, **1983**, pp. 490–560.
- [78] Detection of the molecular peak of the trinuclear complex **1** was always thwarted, whatever the experimental conditions.
- [79] M. T. Caudle, P. J. Riggs-Gelasco, A. K. Gelasco, J. E. Penner-Hahn, V. L. Pecoraro, *Inorg. Chem.* **1996**, *35*, 3577–3584.
- [80] K. Izutsu, *Acid-Base Dissociation Constants in Dipolar Aprotic Solvents, Vol. 35*, Blackwell Scientific Publications, Brookline Village, M. A., **1990**.
- [81] G. M. Sheldrick, *Acta Crystallogr., Sect. A* **1990**, *46*, 467.
- [82] G. M. Sheldrick, *SHELXTL: Program for the Refinement of Crystal Structures*, University of Göttingen, Germany, **1993**.
- [83] G. M. Sheldrick, *SHELXTL*, Version 5.1, University of Göttingen, Germany, **1999**, distributed by Bruker AXS, Madison, WI, USA.

Received: June 3, 2005
Published Online: October 20, 2005